ELSEVIER

Materials Science and Engineering B 123 (2005) 20–30

MATERIALS SCIENCE & ENGINEERING B

www.elsevier.com/locate/mseb

Characterization and process effects of HfO_2 thin films grown by metal-organic molecular beam epitaxy

Myoung-Seok Kim [a], Young-Don Ko [a], Minseong Yun [a], Jang-Hyuk Hong [b], Min-Chang Jeong [b], Jae-Min Myoung [b], Ilgu Yun [a,*]

[a] *Department of Electrical and Electronic Engineering, Yonsei University, 134 Shinchon-Dong, Seodaemun-Gu, Seoul 120-749, Republic of Korea*
[b] *Department of Materials Science and Engineering, Yonsei University, 134 Shinchon-Dong, Seodaemun-Gu, Seoul 120-749, Republic of Korea*

Received 2 October 2004; received in revised form 13 December 2004; accepted 14 June 2005

Abstract

HfO_2 dielectric layers were grown on the p-type Si(1 0 0) substrate by metal-organic molecular beam epitaxy (MOMBE). Hafnium-tetra-butoxide [$Hf(O{\cdot}t\text{-}C_4H_9)_4$] was used as a Hf precursor and argon gas was used as a carrier gas. The microstructure and thickness of HfO_2 films were measured by scanning electron microscopy (SEM) and high-resolution transmission electron microscopy (HRTEM). The electrical characteristics of the HfO_2 layers were evaluated by high frequency (HF) capacitance–voltage (*C*–*V*) and current–voltage (*I*–*V*) measurements. The surface morphology, crystal structure, and chemical binding states of HfO_2 films were also examined by atomic force microscopy (AFM), X-ray diffraction (XRD), and X-ray photoelectron spectroscopy (XPS) measurements. HF *C*–*V* and *I*–*V* measurements have shown that HfO_2 layer grown by MOMBE has higher dielectric constant (*k*) of 20–22 and lower leakage current density of $\sim 10^{-8}$ A/cm^2 compared with the conventional SiO_2. In addition, it has been shown that the HfO_2 layer has fixed oxide charge of about 8×10^{11} cm^{-2} and interfacial state density of about 1×10^{12} eV^{-1} cm^{-2}. The electrical characteristics and surface morphology of HfO_2 films are affected by O_2/Ar gas flow ratio. Finally, post-metallization annealing (PMA) was carried out to reduce the interface state density.
© 2005 Elsevier B.V. All rights reserved.

Keywords: HfO_2; Gate dielectric; Thin film; Electrical property; MOMBE

1. Introduction

The demands of scaling down for complementary metal–oxide–semiconductor (CMOS) technology require the reduction of gate dielectric thickness. With the reduction of gate dielectric thickness to a few nanometers, higher dielectric constant material than the conventional SiO_2 is needed to overcome the problem of an exponential increase in the leakage current level due to direct tunneling. The new insulator should meet the requirements such as high breakdown, low leakage current at operating voltage, low oxide traps, and high thermal stability on silicon. Many researches for high-*k* dielectric constant materials such as ZrO_2, Ta_2O_5, Al_2O_3, HfO_2, TiO_2, silicates ($ZrSi_xO_y$ and $HfSi_xO_y$), and ferroelectric materials [$Pb(Zr,Ti)O_3$ and $(Ba,Sr)TiO_3$] [1–5] have been performed. Among these candidates, HfO_2 is one of the most highlighted high-*k* gate insulators to replace the SiO_2 because of its high dielectric constant (25–30), wide band-gap energy (5.68 eV), high breakdown field (15–20 MV/cm), and good thermal stability on Si substrate. The growth method of high-*k* materials is also an important factor to determine the property of gate dielectric layer. In our experiments, we searched appropriate experimental conditions and examined the characteristics of HfO_2 films using metal-organic molecular beam epitaxy (MOMBE) system. MOMBE is one of the powerful techniques obtaining abrupt interface and controlled thickness of films, mainly due to source evaporation at a controlled rate under ultra high vacuum condition [6]. In this paper, the electrical characteristics of HfO_2 films grown by MOMBE are investigated. The effects of process variation (O_2/Ar ratio and substrate temperature) and post-metallization annealing (PMA) on the properties of HfO_2 films are also analyzed. The electrical

* Corresponding author. Tel.: +82 2 2123 4619; fax: +82 2 313 2879.
E-mail address: iyun@yonsei.ac.kr (I. Yun).

0921-5107/$ – see front matter © 2005 Elsevier B.V. All rights reserved.
doi:10.1016/j.mseb.2005.06.012

characteristics of HfO_2 films are analyzed by high frequency (HF) capacitance–voltage (*C*–*V*) and current–voltage (*I*–*V*) measurements. The film characteristics and surface morphology are examined by using X-ray photoelectron spectroscopy (XPS), scanning electron microscopy (SEM), high-resolution transmission electron microscopy (HRTEM), X-ray diffraction (XRD), and atomic force microscopy (AFM) measurements.

2. Experiment

HfO_2 thin film was grown on a p-type Si(1 0 0) substrate, of which the native oxide was chemically eliminated by (50:1) H_2O:HF solution prior to growth by MOMBE. Hafnium-tetra-butoxide [$Hf(O{\cdot}t\text{-}C_4H_9)_4$] was chosen as the MO precursor because it has a appropriate vapor pressure and relatively low decomposition temperature. High-purity (99.999%) oxygen gas was used as the oxidant. Hf-t-butoxide was introduced into the main chamber using Ar as a carrier gas through a bubbling cylinder. The bubbler was maintained at a constant temperature to supply the constant vapor pressure of Hf-source. The apparatus of the system is schematically shown in Fig. 1. High-purity Ar carrier gas passed through the bubbler containing the Hf-source. The gas line from the bubbler to the nozzle was heated to the same temperature. The mixture of Ar and metal-organic gases heated at the tip of the nozzle flows into the main chamber. The introduced Hf-source decomposed into Hf and ligand parts when it reached a substrate maintained at high temperature and the Hf ion was combined with O_2 gas supplied from another nozzle. The base pressure and working pressure were $\sim 10^{-9}$ and $\sim 10^{-7}$ Torr, respectively. Annealing at 700 °C for 2 min in N_2 ambient was carried out following the growth of the films to diminish the density of the interfacial charged particles [7]. Detailed experimental conditions are listed in Table 1. After metal deposition was performed, the post-metallization annealing (PMA) at 250 °C was carried out in O_2 ambient. In turn, *I*–*V* and HF (1 MHz) *C*–*V* measurements were executed to analyze the electrical characteristics of dielectric layers. To carry out the *I*–*V* characteristics, Keithley 236 source measure unit (SMU) was used. The *C*–*V* measurements were also performed with the Keithley 590 *C*–*V* analyzer at room temperature.

Table 1
Experimental conditions

Process variables	Range
Substrate temperature	300–550 °C
Bubbler temperature	130 °C (fixed)
Nozzle temperatrue	270 °C (fixed)
Base pressure	10^{-9} Torr
Working pressure	10^{-7} Torr
Gas flow (Ar)	2–6 sccm
Gas flow (O_2)	1–8 sccm
Growth time	30 min
Post-metallization annealing temperature	250 °C (in O_2 ambient)

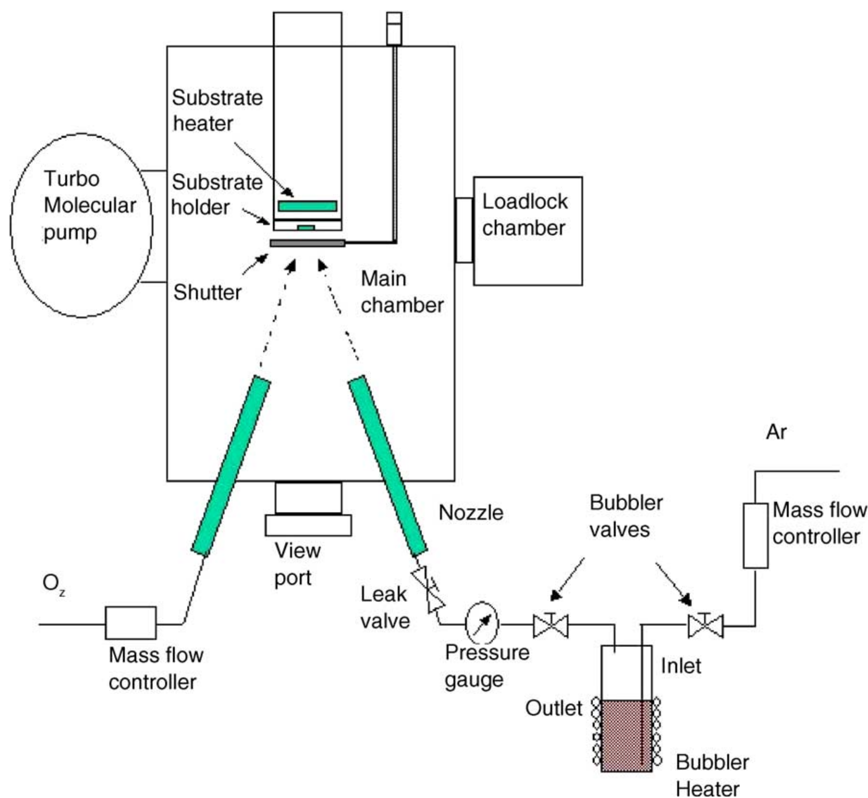

Fig. 1. Schematic illustration of MOMBE system.

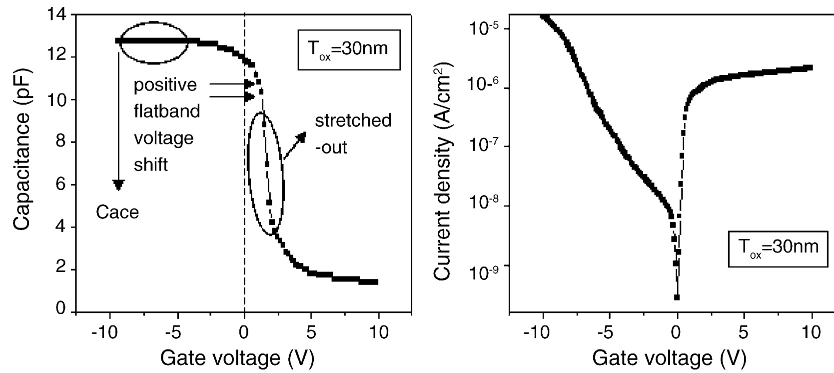

Fig. 2. High frequency *C–V* and *I–V* characteristics of HfO_2 film grown by MOMBE.

3. Results and discussion

The metal–oxide–semiconductor (MOS) capacitor structure Au/HfO_2/p-type Si was fabricated to measure its electrical characteristics. The high frequency (1 MHz) *C–V* curve and *I–V* curve of HfO_2 films grown by MOMBE are shown in Fig. 2. From measured capacitance and physical thickness, the dielectric constant and the equivalent oxide thickness can be obtained. Actually, total capacitance must be calculated as series connection of HfO_2 layer capacitance and SiO_2 layer capacitance because an unexpected SiO_2 layer between HfO_2 and p-Si substrate shown in Fig. 3 affects the total capacitance strongly [8]. The thickness of SiO_2 layers was measured by HRTEM and had a value of 10–20 Å with experimental conditions. It can be identified by TEM images that the formation of SiO_2 was affected by experimental conditions such as the growth time [9], Ar/O_2 gas ratio, and substrate temperature (not shown here). The formation of SiO_2 layer is attributed to the excess oxygen during the film growth and should be eliminated or minimized because of its low dielectric constant. In addition, HfO_2 samples grown at substrate temperature of 400 °C showed an amorphous nature in Fig. 3(a) and (c). However, when the substrate temperature was at 450 °C, a large portion of the HfO_2 film was crystallized and some of the grain boundaries were observed in Fig. 3(b). Ignoring the depletion region effect, the dielectric constant (k = 20–22) can be calculated. This relative low dielectric constant compared with the bulk HfO_2 dielectric constant (k = 25–30) may be

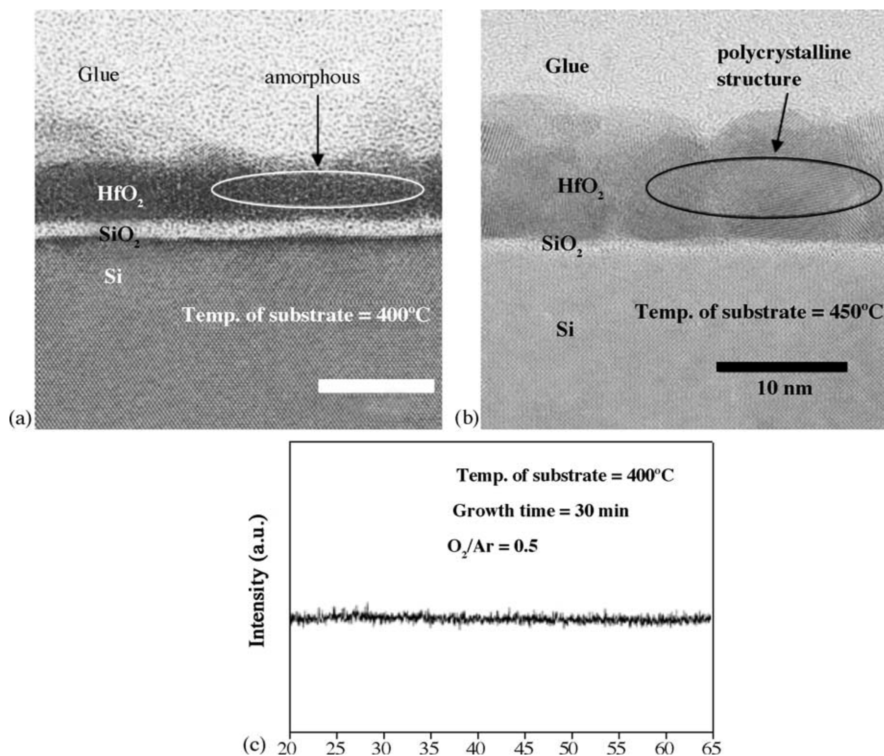

Fig. 3. HRTEM image of HfO_2 film grown by MOMBE (400 and 450 °C).

due to the polycrystalline nature of the grown HfO_2 films and Hf–silicate interfacial layer (not identified in HRTEM image but other research showed that HfO_2/SiO_2 interface are marginally unstable with respect to formation of silicates [10]) that has lower dielectric constant compared with the bulk HfO_2. Generally, the thickness resulted from *C–V* curve is slightly higher than that from TEM. This may be due to two major quantum effects: (i) additional band bending because of surface electrons (or holes) above the edge of conduction band and (ii) presence of charge centroid [7]. The leakage current density of HfO_2 film at positive gate bias (0–2 V) is approximately 10^{-9} A/cm^2 and at negative gate bias (0 to −2 V) is approximately 10^{-7} A/cm^2. Leakage current density of 10^{-9} and 10^{-7} A/cm^2 is a relatively low level compared with that of the conventional SiO_2.

Comparing with an ideal *C–V* curve of a general MOS structure, our curve extracted from experimental data showed positive directed "flat-band voltage shift" and "stretched-out" characteristics. It means that HfO_2 films grown by MOMBE have negative fixed oxide charges and interface traps [11]. The density of fixed oxide charges can be calculated from flat-band voltage shift measurements. The ideal flat-band capacitance of HfO_2 films can be calculated from the following formula [12]:

$$C_{\mathrm{FB}} = \frac{\varepsilon_{\mathrm{f}}}{d + (\varepsilon_{\mathrm{f}}/\varepsilon_{\mathrm{s}})L_{\mathrm{D}}}$$

where ε_f and ε_s are the permittivity of the film and substrate, respectively. In this formula, L_D is the extrinsic Debye length given by

$$L_{\mathrm{D}} = \left(\frac{kT\varepsilon_{\mathrm{s}}}{q^2 N_{\mathrm{a}}}\right)^{1/2}$$

where N_a is the concentration of acceptors in the semiconductor and about 4×10^{15} cm^{-3}. In our experiments, the extrinsic Debye length was about 40 nm. In our HfO_2 films grown by MOMBE, flat-band voltage shift (ΔV_{FB}) varied in the range of 0.7–3.1 V with experimental condition. Fig. 4 showed that the density of fixed oxide charges calculated by flat-band voltage shift (ΔV_{FB}) was about 8×10^{11} cm^{-2}, and not affected by the thickness of film [13]. The density of interface states, D_{it}, was estimated at flat-band voltage (flat-band condition)

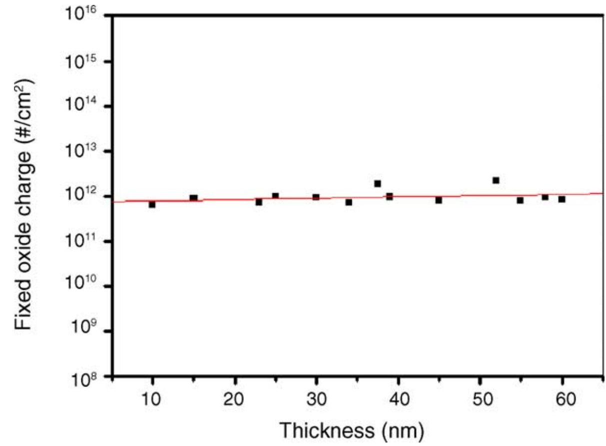

Fig. 4. Fixed oxide charges concentration vs. thickness of HfO_2 film in different experimental conditions.

using Lehovec's method for evaluation of built-in charges from *C–V* plots [14], which gives

$$D_{\mathrm{it}} = \left[\frac{(C_0 - C_{\mathrm{FB}})C_{\mathrm{FB}}}{3(\delta C/\delta V)_{\mathrm{FB}} qkTA}\right] - \left[\frac{C_0^2}{(C_0 - C_{\mathrm{FB}})Aq^2}\right]$$

where *A* is the area of the electrode, *k* the Boltzmann's constant, *T* the absolute temperature, *q* the electron charge, and $(\delta C/\delta V)_{FB}$ is the slope at flat-band voltage. The calculated density of interface states (D_{it}), attributed to the interfacial traps, was approximately 1×10^{12} eV^{-1} cm^{-2}.

The *C–V* characteristics of the films grown at different O_2/Ar ratios are shown in Fig. 5(a). Comparing with the each capacitance in accumulation region, the capacitance at unity O_2/Ar ratio (=1) is lower than other cases. It indicates that the growth rate, film thickness in same growth time, has maximum value when O_2/Ar is unity. In our previous work [15], the growth rate of ZrO_2 films had a maximum value when O_2/Ar ratio was about 1, and the explanation for this phenomenon and statistical modeling were shown. If we remind that HfO_2 and ZrO_2 are II–VI compounds which have similar chemical properties, same explanation may be available for HfO_2 films grown by MOMBE. It could be also identified that as O_2/Ar ratio increased, magnitude of flat-band voltage shift decreased. However, when the O_2/Ar ratio was beyond 1, the

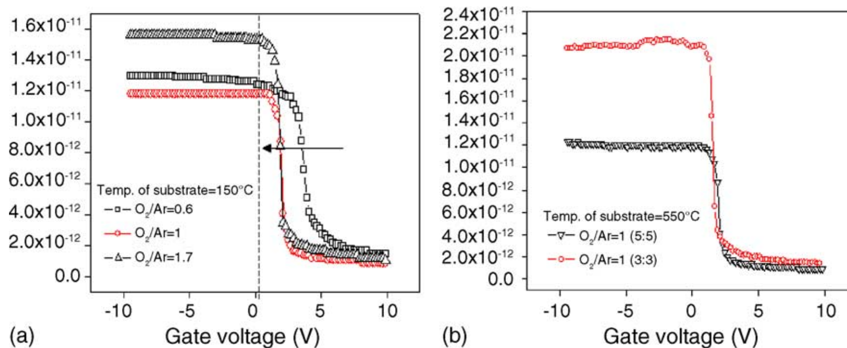

Fig. 5. HF *C–V* characteristics of HfO_2 films grown at different O_2/Ar gas flow ratios and at different gas volume.

flat-band voltage shift did not vary significantly. Smaller flat-band voltage shift indicates a reduction in the density of fixed oxide charges. The density of fixed oxide charge depends on oxidation, annealing condition, and silicon orientation. In addition, it has been suggested that excess silicon (trivalent silicon) or the loss of an electron from excess oxygen centers (nonbridging oxygen) near the Si-oxide interface is the origin of fixed oxide charge [12]. Varying O_2/Ar ratio changed the oxidation condition of HfO_2 and had an influence on the generation of fixed oxide charge in the HfO_2 film. Comparing with the slope of transition region in different O_2/Ar ratio cases, it was observed a steeper slope at higher O_2/Ar ratio (=1.7) than at lower O_2/Ar ratio (=0.6). Steeper slope at the depletion region indicates a decline in the number of interfacial charged particles. So, it can be assumed that large O_2/Ar ratio (or sufficient O_2 gas flow) reduces the density of fixed oxide charges and the number of interfacial charged particles in HfO_2 film grown by MOMBE. The *C–V* characteristics of HfO_2 films at same O_2/Ar ratio but different volume of gas flow is shown in Fig. 5(b). It was observed that flat-band voltage shift was affected significantly not the magnitude of each O_2 and Ar gas flow but the O_2/Ar gas ratio. The slope of transition region at larger gas volume was slightly steeper than that at smaller gas volume. It also indicates that the interfacial trap density is mainly influenced by not the magnitude of O_2 and Ar gas flow but the O_2/Ar ratio. At same O_2/Ar ratio, it was identified that the more gas flows, the higher growth rate.

The *C–V* characteristics of HfO_2 films grown by MOMBE at different substrate temperature are shown in Fig. 6. It was observed that the growth rate of HfO_2 at substrate temperature of 450 °C was higher than that at substrate temperature of 550 °C. It was also observed that the flat-band voltage shift in *C–V* curve increased as the substrate temperature increased.

To examine the effect of the substrate temperature on HfO_2 films, XRD spectra of HfO_2 films grown in a different substrate temperature are shown in Fig. 7. HfO_2 films have been found to exist in monoclinic phase, tetragonal phase, cubic phase, and amorphous structure [16–19]. This crystal structure depends on the growth method and experimental condition of HfO_2 films. It was found that there were monoclinic (m) and tetragonal (t) phase in our HfO_2 films grown at the same annealing condition by MOMBE system, and monoclinic phase (m) was dominant. Through XRD spectra, it was shown that the crystal structure of HfO_2 films was changed with the substrate temperature. At 450 °C, various crystal phase and crystal direction were shown in XRD spectrum. However, at 550 °C, overall XRD spectrum became simple and some peaks disappeared. To investigate the relationship

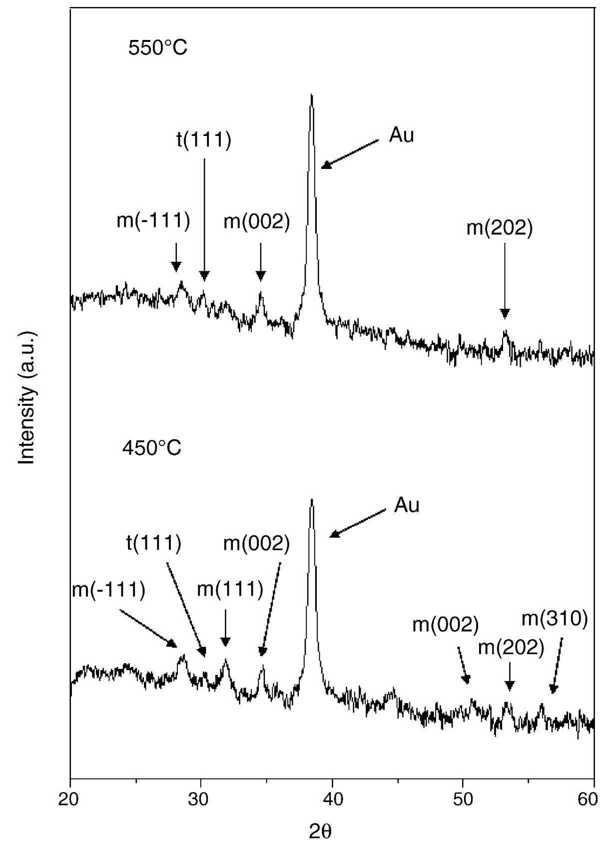

Fig. 7. XRD spectra of HfO_2 films at different substrate temperature: (a) 450 °C and (b) 550 °C.

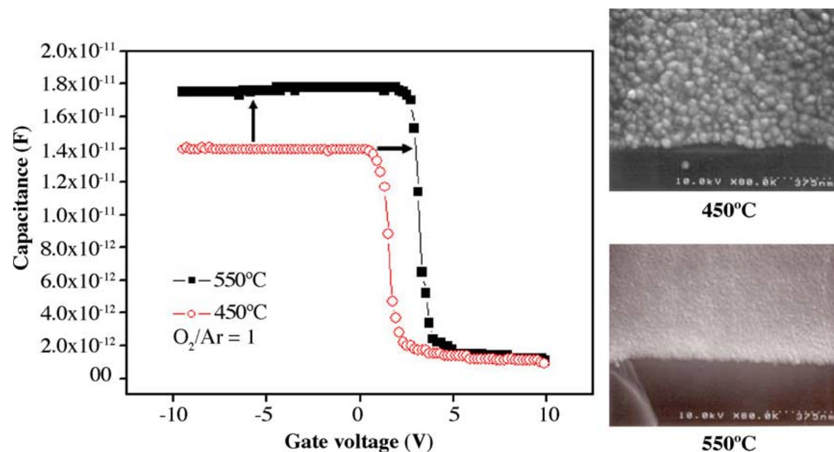

Fig. 6. HF *C–V* characteristics of HfO_2 films grown at different substrate temperature.

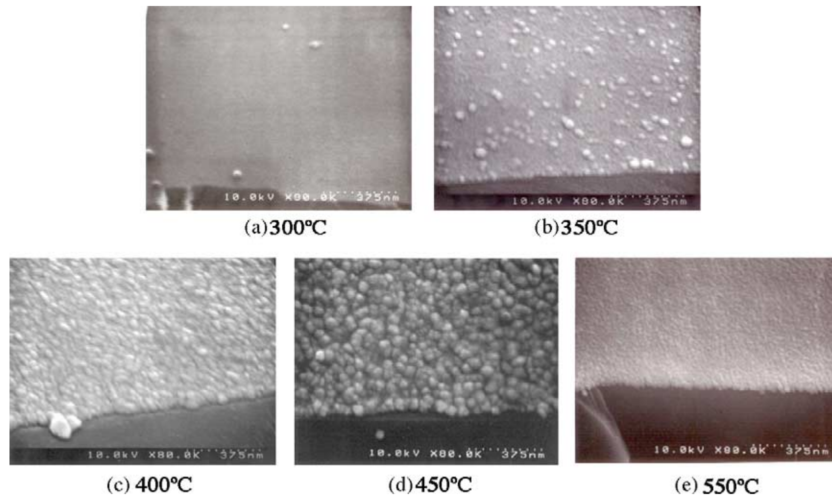

Fig. 8. SEM images of HfO_2 films at different substrate temperature (300, 350, 400, and 450 °C).

between the crystal structure and the substrate temperature more, SEM images of HfO_2 films grown by MOMBE at different substrate temperature (300–550 °C) were shown in Fig. 8. As shown in Fig. 8(a), it was found that HfO_2 film was not grown under the temperature of 300 °C because Hf source was not effectively decomposed. At the temperature of 350 °C, HfO_2 films began to grow, and the crystallization of HfO_2 films was enhanced as the substrate temperature increased, shown in Fig. 8(b), (c) and (d). However, it was found that the crystallite size and degree of crystallization of HfO_2 film were slightly reduced at 550 °C of the substrate temperature shown in Fig. 8(e). Generally, the crystallization of films depends on the growth temperature and film thickness. In our MOMBE system, the HfO_2 film was fully crystallized at substrate temperature of 450 °C, shown in Fig. 8(d). Thus, it can be assumed that the substrate temperature is one of the critical factors changing the crystal structure of HfO_2 films, and also affects the growth rate in our experiments.

It is shown the bi-directional (forward and backward) *C–V* characteristics of HfO_2 films in Fig. 9. It was observed the hysteresis in the bi-directional *C–V* characteristics, and the magnitude of hysteresis decreased as O_2/Ar ratio increased. The hysteresis shown in the *C–V* curve verified that interfacial traps existed in HfO_2 films. An interfacial layer, traps, and mobile ions in thermally grown insulating films may give rise to voltage shift [20,21]. In our experiments, the hysteresis voltage width was not affected by different sweep rates, indicating that the obtained *C–V* curve was in steady state and also suggesting that the present *C–V* hysteresis was caused by interfacial traps [11]. In addition, the clockwise hysteresis in the *C–V* curve indicates a positive carrier injection (or pos-

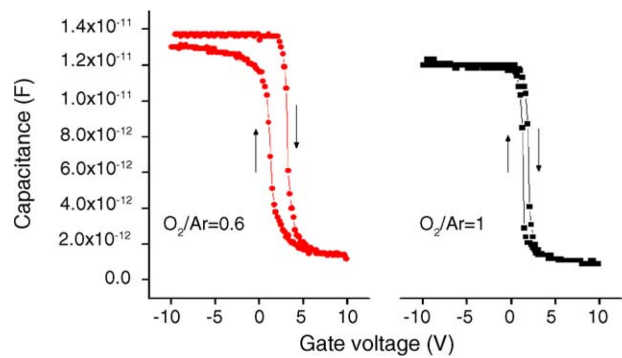

Fig. 9. Bi-directional HF *C–V* characteristics of HfO_2 films at different O_2/Ar gas flow ratios.

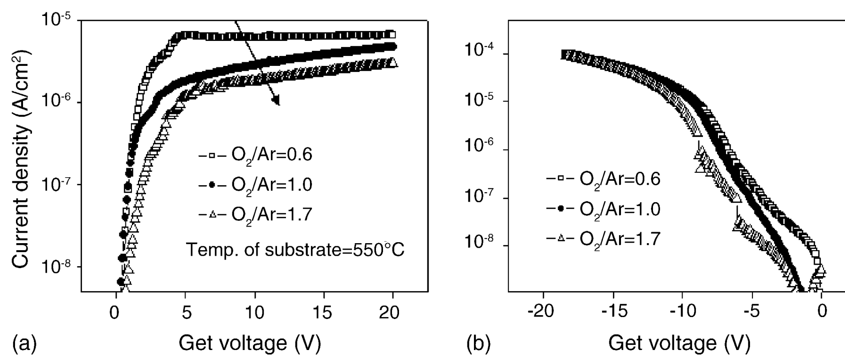

Fig. 10. *I–V* characteristics of HfO_2 films grown at different O_2/Ar gas flow ratios: (a) positive gate voltage and (b) negative gate voltage.

itive trapped charge) into the HfO_2 films [12,22]. The density of state recharged during each bias cycle (N_{it}), i.e. interface states that are occupied and freed by injected and re-emitted charges during each bias cycle, is given by

$$N_{it} = \frac{C_{acc} V_H}{qA}$$

where V_H is the amount of hysteresis during a cycle. In our experiment, it was observed that V_H was about 0.1 V at higher O_2/Ar ratio (≥1), and about 2 V at lower O_2/Ar ratio (≪1). It showed a good agreement with above results that higher O_2/Ar gas ratio reduced the interface state density.

Leakage current densities of HfO_2 films grown by MOMBE in different O_2/Ar gas ratio are shown in Fig. 10. The leakage current at a positive gate voltage decreased with increasing O_2/Ar ratio. In addition, the leakage current in a log scale showed a linear dependence on the square root of gate voltage at all O_2/Ar ratio. This feature is consistent with the Schottky emission mechanism where the charge conduction is dominated by the interface between HfO_2 and Si substrate [23]. Interfacial layer formation increases with increasing O_2/Ar ratio shown in Fig. 11, and it can result in the decrease in the leakage current. At the negative gate voltage region, much higher leakage current was observed, and the leakage current level was invariant as O_2/Ar ratio varied. It indicates that the Au–HfO_2 interface has a high level of defect densities [24]. The difference in the leakage current level between positive and negative gate bias was observed in other HfO_2 films, which were grown in different experimental conditions. The difference is about two orders of magnitude in log scale.

The leakage current density at a different substrate temperature is shown in Fig. 12. The leakage current density increased as the substrate temperature increased. However, more detailed examination about the relationship between the substrate temperature and the leakage current and its physical analysis is needed. It will be remained as our future work.

The surface morphology was strongly affected by the O_2/Ar ratio, as shown in Fig. 13. More smooth HfO_2 films were grown at O_2/Ar = 1.7 (rms = 12.1 Å), while

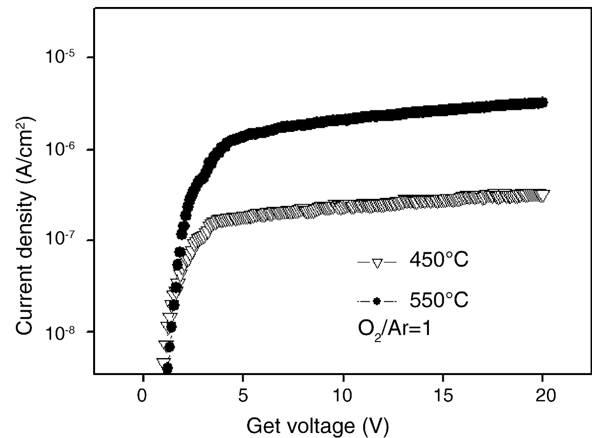

Fig. 12. I–V characteristics of HfO_2 films grown at different substrate temperature.

much rougher HfO_2 films were grown at O_2/Ar = 0.6 (rms = 38.5 Å). In other similar work, the surface morphology of ZrO_2 films grown by PECVD was strongly affected by the O_2/Ar ratio [25]. As the O_2/Ar ratio was varied, an ionic species that dominate the deposition process can be also varied, and it can affect characteristics of HfO_2 films such as dielectric constant, surface morphology, and fixed charge concentration. As shown in Fig. 14, it was also observed that the substrate temperature had an influence on the surface morphology of HfO_2 films grown by MOMBE. Each rms roughness in Fig. 12 was (a) 38.5 Å, (b) 11.6 Å, (c) 12.1 Å, and (d) 5.1 Å, respectively, where each thickness was (a) 43 nm, (b) 50 nm, (c) 35 nm, and (d) 40 nm, respectively. HfO_2 films grown at higher substrate temperature had more smooth surface morphology. In addition, HfO_2 films grown at higher substrate temperature had smaller variation of rms roughness at different O_2/Ar ratio than at lower substrate temperature.

Fig. 15(a) shows the XPS spectra for Hf 4f level that were calibrated from C 1s peak at 284.5 eV. Each spectrum was represented the result at different O_2 gas flow ranging from 2 to 8 sccm and Ar gas flow was fixed at 2 sccm. As shown in Fig. 15(a), the Hf $4f_{5/2}$ and Hf $4f_{7/2}$ peaks, which have binding

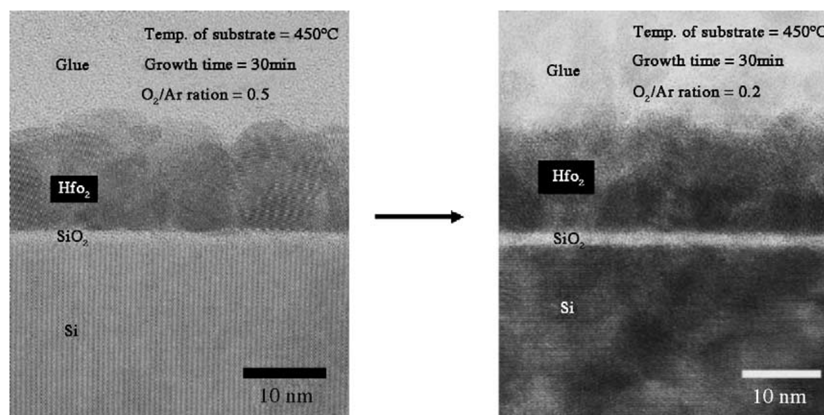

Fig. 11. TEM images of SiO_2 layer in HfO_2 films grown at different O_2/Ar ratio.

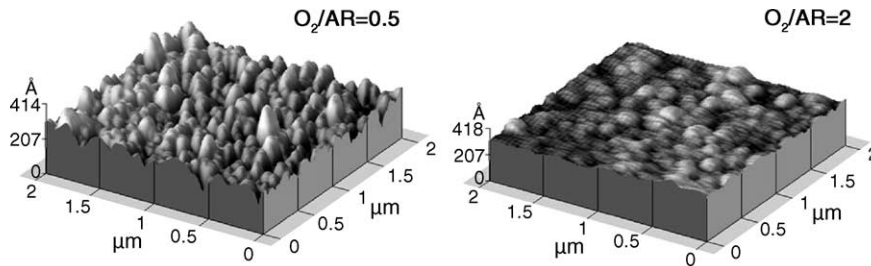

Fig. 13. AFM images of HfO_2 films grown at different O_2/Ar gas flow ratios.

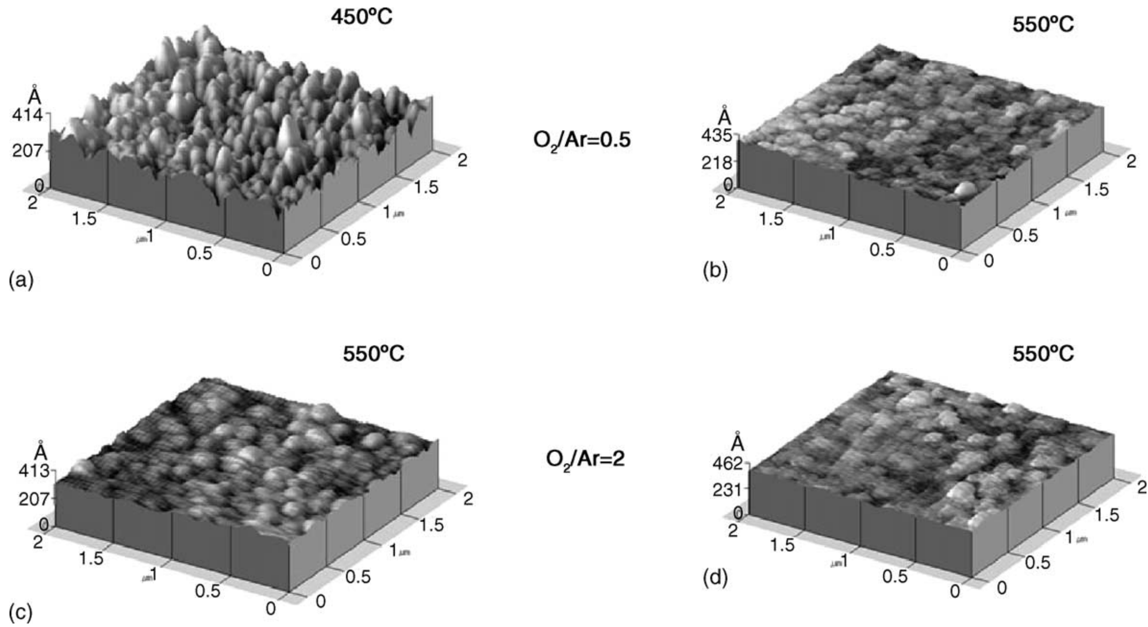

Fig. 14. AFM images of HfO_2 films grown at different O_2/Ar gas flow ratios and substrate temperature.

energies of 16.05 and 17.76 eV, respectively related to Hf–O bonding in HfO_2, shifted to the higher binding energy with increasing of O_2 gas flow. The origins of binding energy shift are suggested as a number of factors such as charge transfer effect, presence of electric field, environmental charge density, and hybridization. Among these, charge transfer is regarded as a dominant mechanism causing a binding energy shift. According to the charge transfer mechanism, removing

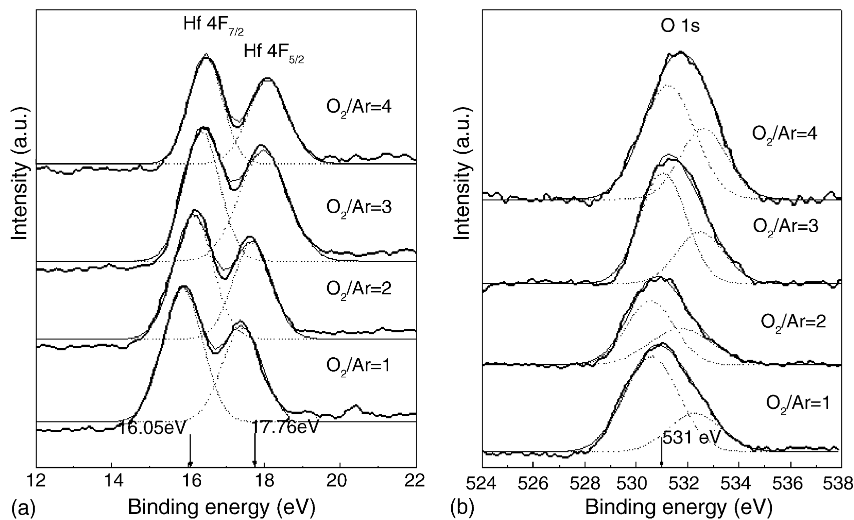

Fig. 15. XPS spectra of HfO_2 film grown by MOMBE: (a) Hf and (b) O.

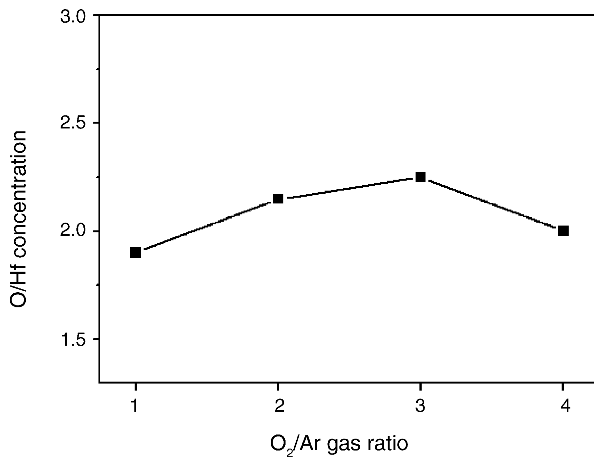

Fig. 16. O/Hf relative concentration at different O_2/Ar gas flow ratios.

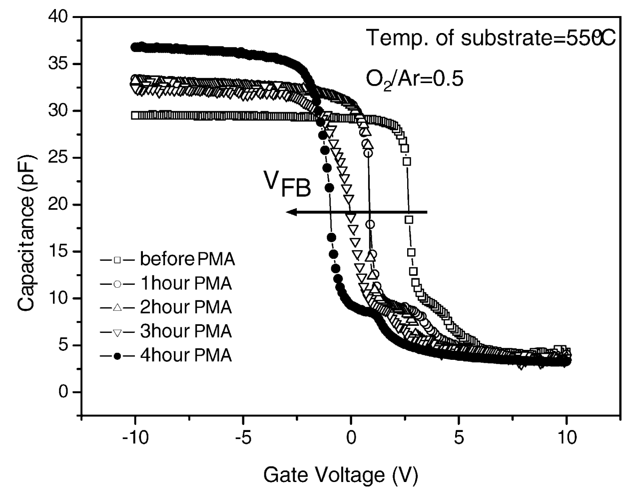

Fig. 18. HF *C–V* characteristic of HfO_2 film before and after PMA process.

an electron from the valence orbital generates the increment in core electron's potential and finally leads a chemical binding energy shift [26]. Therefore, it is considered that the Hf $4f_{5/2}$ and Hf $4f_{7/2}$ peaks shift (ΔBE = 0.6 eV) originated from the enhanced charge transfer with increasing O_2 gas flow, *i.e.*, the larger portion of Hf atoms was fully oxidized with increasing O_2 gas flow. Fig. 15(b) shows the O 1s core level peaks also demonstrated binding energy shift with changing of O_2 gas flow. Each peak can be split into two sub-peaks by Gaussian fitting which represent the Hf–O bonding at ~531 eV and O–C or O–Si bonding at ~532.5 eV [27,28]. The relative quantities of Hf and O elements incorporated in the layer can be obtained by comparing the areas of Hf 4f peak and O 1s sub-peak for Hf–O bonding. Using the atomic sensitivity factors (Hf 4f: 2.221, O 1s: 0.711), the relative concentration ratio (O/Hf) was calculated. The relative concentration ratio (O/Hf) is shown in Fig. 16. It can be inferred that the appropriate stoichiometry can be achieved in our experiments and the relative concentration ratio can be controlled by Ar/O_2 gas ratio.

The *I–V* curves of the HfO_2 film before and after PMA were shown in Fig. 17(a). It was observed that as the annealing time increased, leakage current at the same voltage was increased. It can be explained by the creation of new leaky paths in HfO_2 films during PMA process resulted from the excess thermal energy. The oxide breakdown of the dielectric layer was also examined by *I–V* measurements. As shown in Fig. 17(b), the breakdown is indicated by the sudden increase of the gate leakage currents in the positive voltage region. It was found that increase of the annealing time causes reduction of dielectric breakdown field.

Fig. 18 shows the HF *C–V* characteristics of HfO_2 film before and after annealing treatment. It was observed that the capacitance in accumulation region varied with PMA time. Variation of accumulation capacitance can be interpreted as the change of dielectric constant [29], the creation of Hf–silicate layer, or the variation in film thickness [30]. However, in our PMA experiment the temperature is fixed at 250 °C, which is relatively low temperature to change the dielectric constant of a bulk HfO_2. Therefore, it can be assumed that the change in accumulation capacitance indicates the reduction of the oxide layer thickness and the creation of Hf–silicate layer. As shown in other previous work [31], the annealing process may give rise to the reduction of film thickness, which is identified by TEM. It shows that thermal energy in the annealing process enhances the crystalline nature of the films and makes the films denser. In addition, as indicated in other reference [32], the variation in accumulation capacitance can be due to the formation of Hf-silicate

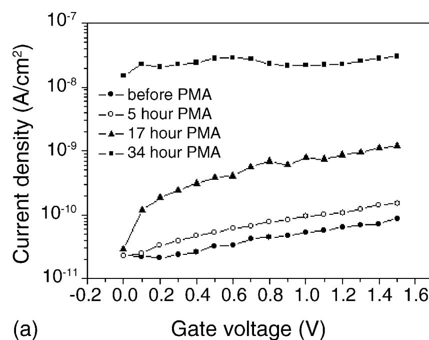

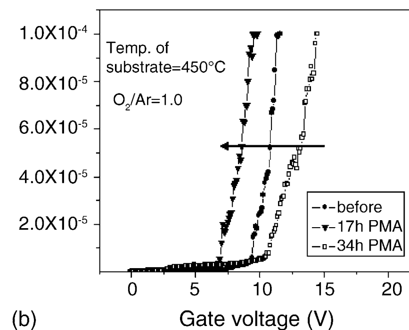

Fig. 17. Leakage current density and breakdown field of HfO_2 film before and after PMA process.

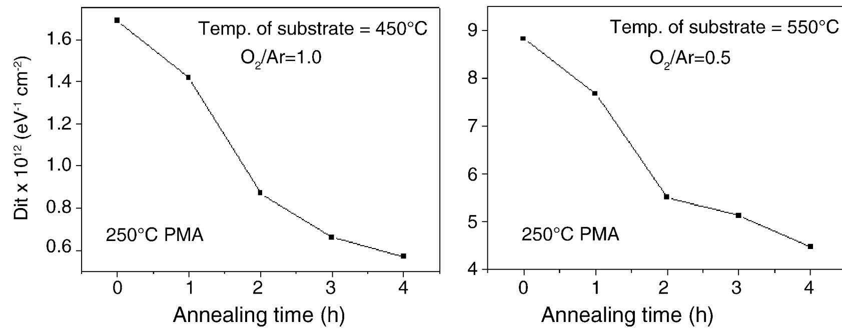

Fig. 19. Interface state density versus the PMA process time of HfO_2 film.

($HfSi_xO_y$) which has relatively low dielectric constant compared with HfO_2 films. In addition, flat-band voltage shift (ΔV_{FB}) was reduced as PMA time increased, suggesting that PMA treatment reduces the oxide charges in HfO_2 layer.

The decrease of interface state density was observed with increasing the annealing time, shown in Fig. 19. It implies that the quality of the interfacial layer of HfO_2 seems to be improved by the annealing. It is attributed to reduction of the number of oxygen vacancy as the annealing time increases. Since oxygen vacancies often act as shallow donors in oxide layer, annealing in O_2 ambient removes oxygen vacancies in the layer [31]. Here, the PMA treatment can be considered as another reason for the reduction of stress in oxide layer. The formation of interface trap is affected by the reaction between the hot electrons and weak bonds in HfO_2/Si. These weak bonds can be induced from the existing stress of Hf–O bonds in HfO_2/Si. Thus, the PMA treatments can reduce the existing stress in oxide layer, and cause the reduction in interface state density.

4. Conclusion

The characteristics of the HfO_2 dielectric layer on the p-type Si substrate by MOMBE process were investigated. The calculated dielectric constant (k = 20–22) was lower than the expected value, known bulk dielectric constant (25–30). Based on the C–V curve of HfO_2 films grown by MOMBE, negative fixed oxide charges and interface traps in the film were examined. Through bi-directional C–V curve, the existence of interface traps can be identified by hysteresis. As the O_2/Ar gas ratio increased, the density of interface states and negative fixed charges decreased. It was also observed that the surface morphology was improved as O_2/Ar ratio increased. In addition, it was observed that the crystal structure was affected by the substrate temperature. It was revealed that the HfO_2 film grown by MOMBE had monoclinic and tetragonal phase. It could be also identified that the leakage current level was decreased with increasing the O_2/Ar gas ratio at a positive gate bias. Finally, post-metallization annealing reduced the interface state density and flat-band voltage shift in the HfO_2 films. However, PMA process increased the leakage current level and reduced the breakdown field strength.

Acknowledgements

This research was supported by the MIC (Ministry of Information and Communication), Korea, under the ITRC (Information Technology Research Center) support program supervised by the IITA (Institute of Information Technology Assessment).

References

[1] M. Copel, M. Gribelyuk, E. Gusev, Appl. Phys. Lett. 76 (4) (2000) 436.
[2] G.B. Alers, R.M. Fleming, Y.H. Wong, B. Dennis, A. Pinczuk, G. Redinbo, R. Urdahl, E. Ong, Z. Hasan, Appl. Phys. Lett. 72 (11) (1998) 1308.
[3] Stefan Jakschik, Uwe Schroeder, Thomas Hecht, Dietmar Krueger, Guenther Dollinger, Andreas Bergmaier, Claudia Luhmann, Johann W. Bartha, J. Appl. Surf. 211 (2003) 352.
[4] Q. Fang, J.Y. Zhang, Z.M. Wang, J.X. Wu, B.J. O'Sullivan, P.K. Hurley, T.L. Leedham, H. Davies, M.A. Audier, C. Jimenez, J.-P. Senateur, W. Boyd Ian, Thin Solid Films 427 (2003) 391.
[5] J.P. Chang, Y.S. Lin, Appl. Phys. Lett. 79 (22) (2001) 3666.
[6] G.B. Stringfellow, Organometallic Vapor-Phase Epitaxy: Theory and Practice, 2nd ed., Academic Press, San Diego, USA, 1999.
[7] Alvin Chi-hai Ng, Jun Jun Xu, J.B. Xu, W.Y. Cheung, Proceedings of the Electron Device Meeting, IEEE, Hong Kong, 2001, p. 101.
[8] G.D. Wilk, R.M. Wallace, J.M. Anthony, J. Appl. Phys. 89 (2001) 5243.
[9] T. Moon, M. Ham, M. Kim, I. Yun, J. Myoung, Appl. Surf. Sci. 240 (2005) 105.
[10] Maciej Gusowski, John E. Jaffe, Chun-Li Liu, Matt Stoker, Rama I. Hegde, Raghaw S. Rai, Philip J. Tobin, Appl. Phys. Lett. 80 (11) (2002) 1897.
[11] E.H. Nicollian, J.R. Brews, MOS (Metal–Oxide–Semiconductor) Physics and Technology, Wiley/Interscience, 1981.
[12] S.M. Sze, Physics of Semiconductor and Devices, 2nd ed., Wiley/Interscience, 1981.
[13] W.S. Lindenberger, A.R. Tretola, W.D. Powell, A.K. Sinha, Solid State Electron. 23 (1980) 1179.
[14] K. Lehovec, A. Slobodskoy, Solid State Electron. 7 (1964) 59.
[15] M. Kim, Y. Ko, J. Hong, M. Jeong, J. Myoung, I. Yun, Appl. Surf. Sci. 227 (2004) 387.

[16] M. Alvisi, S. Scaglione, S. Martelli, A. Rizzo, L. Vasanelli, Thin Solid Films 354 (1999) 19.
[17] K. Kukli, J. Ihanus, Appl. Phys. Lett. 68 (1996) 3737.
[18] J. Wang, J. Mater. Sci. 27 (1992) 5397.
[19] J. Aarik, A. Aidla, Appl. Surf. Sci. 173 (2001) 15.
[20] T. Sawada, H. Hasegawa, Thin Solid Films 56 (1979) 183.
[21] E.H. Snow, A.S. Grove, B.E. Deal, C.T. Sah, J. Appl. Phys. 36 (1965) 1664.
[22] Q.X. Jia, Z.Q. Shi, W.A. Anderson, Thin Solid Films 209 (1992) 230.
[23] J.R. Yeargan, H.L. Taylor, J. Appl. Phys. 39 (1968) 5600.
[24] B.O. Cho, J. Wang, L. Sha, J.P. Chang, Appl. Phys. Lett. 80 (2002) 1052.
[25] B.O. Cho, J. Wang, C.P. Chang, J. Appl. Phys. 92 (2002) 4238.
[26] P.S. Bagus, F. Illas, G. Paccghioni, F. Parmigiani, J. Electron Spectrosc. Related Phenom. 100 (1999) 215.
[27] H.Y. Yu, X.D. Feng, D. Grozea, Z.H. Lu, R.N.S. Sodhi, A.M. Hor, H. Aziz, Appl. Phys. Lett. 78 (2001) 2595.
[28] J.P. Chang, Y.S. Lin, J. Appl. Phys. 90 (2001) 2964.
[29] N. Zhan, K.L. Ng, H. Wong, M.C. Poon, C.W. Kok, Proceedings of the 2003 IEEE Conference on Electron Devices and Solid-State Circuits, 2003, p. 431.
[30] Asuha, T. Yuasa, O. Maida, H. Kobayashi, Appl. Phys. Lett. 80 (2002) 4175.
[31] G.D. Wilk, D.A. Muller, Appl. Phys. Lett. 83 (2003) 3984.
[32] J.P. Chang, Y.S. Lin, Appl. Phys. Lett. 79 (2001) 3666.